

USPAS 2008, University of Maryland

PHASE SPACE TOMOGRAPHY LECTURE NOTES¹

Prepared By

Diktys Stratakis

Instructor for the UMER course for USPAS 2008
Institute for Research in Electronics and Applied Physics,
University of Maryland, College Park, MD 20742

¹All lecture notes are from the following Dissertation: D. Stratakis, Ph.D. Dissertation, "Tomographic Measurement of the Phase Space Distribution of a Space-Charge-Dominated Beam", University of Maryland, 2008

© Copyright by
Diktys Stratakis
2008

Tomography Theory

Measurement of the transverse phase space distribution is an important tool to understand transverse particle dynamics in accelerators. Standard methods that are commonly used in the accelerator community to map the beam phase space (such as the quadrupole scan, pepper pot, and slit wire scan) were briefly reviewed in Chap. 1 and as it was evident they had some limitations. Therefore, it is advantageous to develop new methods to accurately reconstruct the beam phase space.

This chapter describes how to measure the transverse phase space distribution by combining the ideas of quadrupole-scanning with Tomographic image techniques. Prior work demonstrated that it is possible to map the beam phase space by measuring spatial projections of the beam. However, these previous methods were applied to relativistic beams with no space-charge. In this chapter we discuss the difficulties arising in cases where space-charge is present and demonstrate an algorithm for Tomographic phase space mapping for intense space-charge dominated beams.

The outline of this chapter is as follows: In Sec. 2.1 we briefly review the basic beam theory, discuss the motion of a single beam particle and define space-charge. In Sec. 2.2 we review the tomography algorithm and its relations to the phase space measurement for beams without space-charge. In Sec. 2.3 we show the extension algorithm to use tomography to beams with space-charge. In Sec. 2.4 we discuss the modifications we do to apply the diagnostic for our experiments. Finally, we review the image analysis software for tomography and show a step by step example where we describe how to use it to reconstruct the beam phase-space.

2.1 Basic Theory

A beam consists of a group of particles that have small energy spread compared to their average translational energy, and where the particle transverse motion is at very small angles with respect to the beam translational orbit. We briefly review the motion of a single beam particle and discuss the implications when space-charge is present.

2.1.1 Beam Transfer Matrices

In this section we describe the transverse particle motion at the exit of a beam transport location, such as a lens or a simple drift segment, relative to the orbit at the entrance. As discussed in Chap.1 the position of the particle can be represented as a point in a six dimensional space. Assume that the beam propagates in the z-direction with a longitudinal momentum and size much higher than the momentum and size in the transverse directions. Then, the transverse particle orbit at some axial position can be represented by the four-dimensional vector (x, x', y, y') , where x (or y) is the transverse displacement from the horizontal plane x (or y). The quantity x' (or y') is the angle the particle makes in that plane with respect to the main axis z . In many practical cases the forces in the x and y directions are independent and we can calculate the particle motion in x and y separately using the two-dimensional vectors (x, x') and (y, y') , respectively. We shall concentrate our analysis of orbits that are separable in x and y .

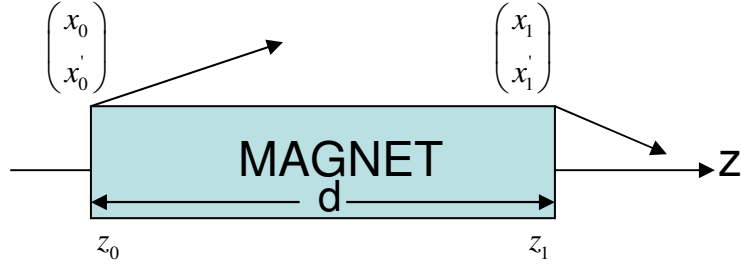


Figure 0.1: Layout showing a particle that enters a lens at z_0 and exits the lens at z_1 .

Consider the motion of a particle along the transverse x -direction in a lens of length d as shown in Fig. 2.1. If the exit vector is (x_1, x'_1) and the entrance vector is (x_0, x'_0) then the particle equation of motion is:

$$\frac{d^2 x}{dz^2} = -\kappa_0 x, \quad (2.1)$$

where $F = \kappa_0 x$ is the focusing force of the lens assumed to be linear. Equation 2.1 has the following solutions:

$$x_1 = x_0 \cos(\sqrt{\kappa_0} d) + \frac{x'_0}{\sqrt{\kappa_0}} \sin(\sqrt{\kappa_0} d), \quad (2.2)$$

$$x'_1 = -x_0 \sqrt{\kappa_0} \sin(\sqrt{\kappa_0} d) + x'_0 \cos(\sqrt{\kappa_0} d). \quad (2.3)$$

In matrix notation, the above equations can be written as:

$$\begin{pmatrix} x_1 \\ x'_1 \end{pmatrix} = \begin{pmatrix} \cos(\sqrt{\kappa_0} d) & \frac{1}{\sqrt{\kappa_0}} \sin(\sqrt{\kappa_0} d) \\ -\sqrt{\kappa_0} \sin(\sqrt{\kappa_0} d) & \cos(\sqrt{\kappa_0} d) \end{pmatrix} \begin{pmatrix} x_0 \\ x'_0 \end{pmatrix} = T \begin{pmatrix} x_0 \\ x'_0 \end{pmatrix}. \quad (2.4)$$

The matrix T is known as the *transport matrix* of the lens and κ_0 is often called the *focusing function* and is related to the strength of the lens. For quadrupole magnets the focusing function is [7]

$$\kappa_0 = \frac{qg}{m\gamma\beta c}, \quad (2.5)$$

where g is the quadrupole field gradient; q , m , and c are the particle charge, mass and speed of light, respectively. In practice, it is common to model the quadrupole by using a “hard-edge” approximation where the magnetic field is constant inside the quadrupole over a certain length, known as effective length L_{eff} , and drops to zero outside. From Eq. 2.2 we see that particles oscillate harmonically when traveling through the lens. Those oscillations are known as *betatron oscillations* with *betatron wavelength*, $\lambda_{\beta 0}$, which for our case is $\lambda_{\beta 0} = 2\pi / \sqrt{\kappa_0}$.

As it easy follows from Eq. 2.4 when the beam is passing through a drift section (κ_0 is zero), the transport matrix becomes

$$T = \begin{pmatrix} 1 & d \\ 0 & 1 \end{pmatrix}. \quad (2.6)$$

Next, we are interested to study the influence of space-charge on the particle motion.

2.1.2 Space-charge Effects on Particle Motion

In the previous chapter we assumed that individual particles are moving only under the influence of the external focusing forces. However, as the current is increased the superimposed electric field generated by the particles themselves becomes non-negligible generating phenomena known as space-charge (see Sec. 1.3).

Space-charge results to a repelling force, F_{SC} , and therefore Eq. 2.1 becomes

$$\frac{d^2x}{dz^2} = -\kappa_0 x + F_{SC}. \quad (2.7)$$

Space-charge force has been shown to be linear for uniform distributions [7]. Then, Eq. 2.7 can be written as

$$\frac{d^2x}{dz^2} = -\kappa_0 x + \frac{Kx}{R(z)^2} = \kappa x, \quad (2.8)$$

where $R(z)$ is the radius assumed that the beam is round; K is the generalized beam perveance a unitless quantity that depends on the beam current and is given by [7]

$$K = \frac{qI}{2\pi\epsilon_0 m v^3}, \quad (2.9)$$

where I is the current; v is the velocity of the beam; and ϵ_0 is the permittivity. As we can see from Eq. (2.8) space charge decreases the focusing efficiency of the lens by a factor of $K/R(z)^2$. This leads to an increase of the amplitude of the particle oscillations and the particles are said to perform *depressed betatron oscillations* with a wavelength $\lambda_\beta = 2\pi/\sqrt{\kappa}$.

It is often more convenient to describe the average beam evolution by using rms quantities. Then, the beam transport for an axisymmetric channel is governed by the 2-D rms envelope equations [38]

$$\frac{d^2 \bar{R}(z)}{dz^2} + \kappa_0 \bar{R}(z) - \frac{K}{\bar{R}(z)} - \frac{\epsilon^2}{\bar{R}(z)^3} = 0, \quad (2.10)$$

where \bar{R} is $2 \times rms$ beam radius and ϵ is the $4 \times rms$ emittance. One of the advantages of using the beam envelope equations is that even though they are proven for a beam with a uniform distribution ($\bar{R} = R$) they can describe the evolution of nonuniform

beams as long as they energy, current, rms size and divergence are equivalent to that of a uniform beam [7, 38].

From Eq. (2.10) we can see that the average behavior of the beam is determined by three forces: the focusing force, the space charge force and the thermal pressure force from the emittance. When these forces are balanced

$$\kappa_0 \bar{R}(z) = \frac{K}{R(z)} + \frac{\epsilon^2}{R(z)}, \quad (2.11)$$

and the beam is known as *matched*. Depending on which of the two terms in the right side of Eq. (2.11) dominate, the beam is space-charge dominated ($\frac{K}{R} > \frac{\epsilon^2}{R}$) or

emittance-dominated ($\frac{K}{R} < \frac{\epsilon^2}{R}$).

Another way to quantify space-charge is by introducing the dimensionless intensity parameter χ which can be expressed as the ratio of space-charge force to external focusing force and is given by [39]

$$\chi = \frac{K}{\kappa_0 R}. \quad (2.12)$$

If, $0 < \chi \leq 0.5$ the beam is emittance dominated, if $0.5 < \chi < 1$ it is space charge dominated. The betatron wavelength and depressed wavelength can be expressed in terms of the intensity parameter χ by

$$\frac{\lambda_\beta}{\lambda_{\beta 0}} = (1 - \chi)^{-1/2}. \quad (2.13)$$

Clearly, as χ approaches unity the betatron wavelength becomes extremely large.

2.2 Tomography for Beams without Space-Charge

We now review the tomography algorithm (Sec. 2.2.1) and show its extension to reconstruct the beam phase space distribution (Sec. 2.2.2).

2.2.1 Filtered-Backprojection Algorithm

Several algorithms [40] are available to compute high quality reconstructions from projection data, e. g., Algebraic Reconstruction Technique, Maximum Entropy Tomography, filtered-backprojection algorithm (FBA), etc. The FBA algorithm is the most common method to reconstruct a two-dimensional image and is generally believed that it provides a reconstructed image of high quality with normally available computer capacity and computational times [40]. This is the algorithm that we use and hence we describe in detail along the lines below.

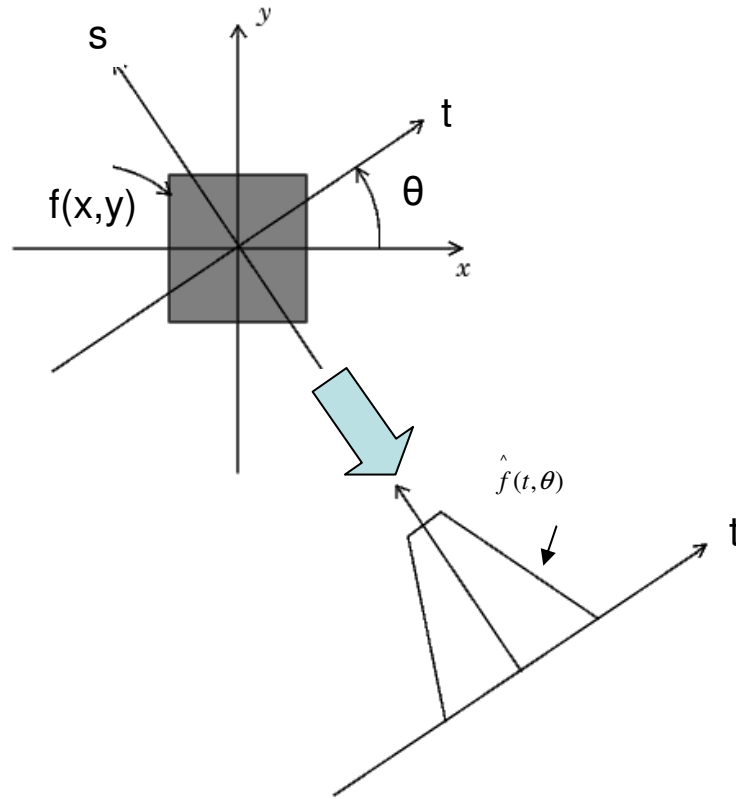


Figure 0.2: Illustration of the Radon Transform

Suppose that $f(x, y)$ corresponds to a two dimensional distribution. Then the integral

$$\hat{f}(t, \theta) = \int_{-\infty}^{\infty} \int_{-\infty}^{\infty} dx dy f(x, y) \delta(x \cos \theta + y \sin \theta - t) \quad (2.14)$$

defines the transverse projection of the distribution $f(x, y)$ along the axis $t = x \cos \theta + y \sin \theta$, placed at an angle θ relative to the x-axis. Such a projection is known as the *Radon transform* of the function $f(x, y)$ and is shown in Fig. 2.2. If $F(u, v)$ is the two-dimensional Fourier transform of the function $f(x, y)$, then its inverse Fourier transform is given by

$$f(x, y) = \int_{-\infty}^{\infty} \int_{-\infty}^{\infty} F(u, v) e^{j2\pi(ux+vy)} dudv. \quad (2.15)$$

By exchanging the rectangular coordinate system in the frequency domain (u,v) for a polar coordinate system (w, θ) Eq. (2.15) becomes

$$f(x, y) = \int_0^{\pi} \int_{-\infty}^{\infty} F(w, \theta) |w| e^{j2\pi wt} dw d\theta. \quad (2.16)$$

Likewise, the Fourier transform of the Radon transform is

$$S(w, \theta) = \int_{-\infty}^{\infty} \hat{f}(t, \theta) e^{-j2\pi wt} dt. \quad (2.17)$$

Using the Fourier Slice Theorem [40] we can write $F(w, \theta) = S(w, \theta)$ and therefore

$$f(x, y) = \int_0^{\pi} \int_{-\infty}^{\infty} S(w, \theta) |w| e^{j2\pi wt} dw d\theta, \quad (2.18)$$

or simpler

$$f(x, y) = \int_0^{\pi} Q(t, \theta) d\theta, \quad (2.19)$$

where Q is given by

$$Q(t, \theta) = \int_{-\infty}^{\infty} S(w, \theta) |w| e^{j2\pi wt} dw, \quad (2.20)$$

and is called “filtered projection” [40]. Therefore, if a number of projections between 0 and π are known, the distribution can be reconstructed by backprojecting the filtered version of the projections according to Eq. (2.19).

2.2.2 Extension of Tomography to Beam Physics

Now, we will show that beam images in configuration space are related by a simple scaling equation to projections of the phase space distribution. The idea is the following: As discussed in Sec 2.1.1 the transverse beam evolution can be described by a 4-dimensional phase space distribution $\mu(x, x', y, y')$. Placing a screen along the beam path gives a two dimensional projection of this distribution, known as the *configuration space*, and is given by

$$g(x, y) = \iint \mu(x, x', y, y') dx' dy' . \quad (2.21)$$

Integration over y leads to the beam profiles along x

$$c(x) = \int g(x, y) dy = \iiint \mu(x, x', y, y') dx' dy' dy . \quad (2.22)$$

We are interested to reconstruct the 2-dimensional phase space distribution $\mu(x, x')_z$ at a particular z , which is given by

$$\mu(x, x')_z = \iint \mu(x, x', y, y') dy dy' . \quad (2.23)$$

The corresponding spatial projection of this distribution is

$$h(x) = \int \mu(x, x')_z dx' = \iiint \mu(x, x', y, y') dy dy' dx' . \quad (2.24)$$

From Eq. (2.22) and Eq. (2.24) we can see that

$$c(x) = h(x) \quad (2.25)$$

Therefore, the beam profile obtained from the integration of the distribution along y is equivalent to the spatial projection of the phase space distribution.

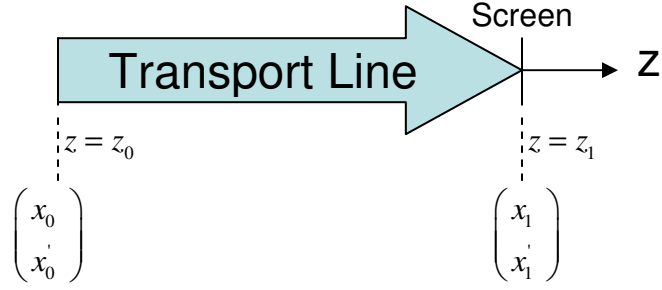


Figure 0.3: Schematic layout of the beam transport line. The starting location is at z_0 and ending location is at z_1 .

Suppose that our beam transport line is that shown in Fig. 2.3. Then, if $g(x_1, y_1)_{z_1}$ is the beam distribution at a location z_1 downstream, according to Eq. 2.25 we can write

$$c(x_1) = \int g(x_1, y_1)_{z_1} dy_1 = h(x_1) = \int \mu(x_1, x_1')_{z_1} dx_1', \quad (2.26)$$

where $\mu(x_1, x_1')_{z_1}$ is the 2-D phase distribution at z_1 . Using the Dirac delta function, it can be written in the equivalent form

$$c(x) = \int \int \mu(x_1, x_1')_{z_1} \delta(x_1 - x) dx_1 dx_1', \quad (2.27)$$

where x is a point within the beam distribution at z_1 . According to Liouville's theorem [7] the particle density remains constant, therefore

$$\mu(x_0, x_0')_{z_0} = \mu(x_1, x_1')_{z_1}, \quad (2.28)$$

where $\mu(x_0, x_0')_{z_0}$ is the 2D phase space distribution at the starting location z_0 . If we assume that we have a linear system, the particle motion between z_0 and z_1 obeys

$$\begin{pmatrix} x_1 \\ x_1' \end{pmatrix} = M_1 \begin{pmatrix} x_0 \\ x_0' \end{pmatrix}, \quad (2.29)$$

where $M_1 = \begin{pmatrix} M_{11} & M_{12} \\ M_{21} & M_{22} \end{pmatrix}$ is the transport matrix. Typically the transport line can consist of drift sections and several lenses. By combining Eq. (2.28) with Eq. (2.29) we can write:

$$c(x) = \iint \mu(x_0, x'_0)_{z_0} \delta(M_{11}x_0 + M_{12}x'_0 - x) dx_0 dx'_0. \quad (2.30)$$

In order to relate Eq. (2.30) to the Radon transform we define the scaling factor, s , by [21]

$$s = \sqrt{M_{11}^2 + M_{12}^2}, \quad (2.31)$$

and the phase space rotation angle θ , by [21]

$$\tan \theta = \frac{M_{12}}{M_{11}}. \quad (2.32)$$

Now, using Eq. (2.31) and Eq. (2.32), Eq. (2.30) becomes

$$c(x) = \frac{1}{s} \iint \mu(x_0, x'_0)_{z_0} \delta(x_0 \cos \theta + x'_0 \sin \theta - \rho) dx_0 dx'_0, \quad (2.33)$$

where $\rho = x/s$.

Comparing Eq. (2.14) with Eq. (2.33) we can write

$$\hat{\mu}(\rho, \theta)_{z_0} = \hat{\mu}(x/s, \theta)_{z_0} = sc(x/s). \quad (2.34)$$

From Eq. (2.34) we can deduce that a simple scaling equation relates the spatial beam projections to the Radon transform, $\hat{\mu}(x/s, \theta)_{z_0}$ of the transverse phase space. This is a very useful result since the beam spatial distribution can be easily obtained in experiments, e.g., using a phosphor screen. Both, scaling factor and

angles of the projection can be easily calculated from the beamline overall transport matrix and are functions of the magnet focusing.

The complete beam tomography procedure can therefore be as follows:

For a given magnet setting:

1. Calculate the transport matrix M_1 between z_0 and z_1
2. At point $z = z_1$, get the beam distribution $g(x, y)$ and calculate the profile by using Eq. 2.26.
3. Calculate the rotation angle and scaling factor by using Eq. 2.31 and Eq. 2.32
4. Relate the beam profile to the Radon transform by scaling the profile vertically by s and horizontally by x/s according to Eq. 2.34
5. Filter the projections by calculating Q from Eq. 2.20
6. Change the magnet setting and repeat steps 1-5

At the end of the scan integrate the filtered projections, Q , over the rotation angle by using Eq. 2.19.

2.2.3 Example: Tomography with Quadrupoles

In the previous section we studied theoretically how to relate the beam profiles to the Radon transform of the phase space. Here we are interested to demonstrate an example of this process. Suppose that the transport line of Fig. 2.3 consist of a quadruple lens of effective length L_1 followed by a drift section of length L_2 . Such configuration is illustrated in Fig. 2.4.

Our goal is to measure the phase space at z_0 by collecting beam profiles at z_1 . We will follow step by step the process described in section 2.2.2. First, we have to calculate the transfer matrix M_1 . For our beamline

$$M_1 = M_D M_Q, \quad (2.35)$$

where M_D is the transport matrix of the drift section given by Eq. (2.6) and M_Q is the transport matrix of the quadrupole given by Eq. (2.4). By multiplying those matrices we get

$$M_1 = \begin{pmatrix} -L_2 \sqrt{\kappa_0} \sin(\sqrt{\kappa_0} L_1) + \cos(\sqrt{\kappa_0} L_1) & \frac{1}{\sqrt{\kappa_0}} \sin(\sqrt{\kappa_0} L_1) + L_2 \cos(\sqrt{\kappa_0} L_1) \\ -\sqrt{\kappa_0} \sin(\sqrt{\kappa_0} L_1) & \cos(\sqrt{\kappa_0} L_1) \end{pmatrix}. \quad (2.36)$$

Next, we can use this information to get the rotation angle and scaling factors. Hence, by using Eq. (2.32) the rotation angle is

$$\theta = \tan^{-1} \left(\frac{\frac{1}{\sqrt{\kappa_0}} \sin(\sqrt{\kappa_0} L_1) + L_2 \cos(\sqrt{\kappa_0} L_1)}{-L_2 \sqrt{\kappa_0} \sin(\sqrt{\kappa_0} L_1) + \cos(\sqrt{\kappa_0} L_1)} \right), \quad (2.37)$$

and from Eq. (2.31) the scaling factor is

$$s = \sqrt{\left[\frac{1}{\sqrt{\kappa_0}} \sin(\sqrt{\kappa_0} L_1) + L_2 \cos(\sqrt{\kappa_0} L_1) \right]^2 + \left[-L_2 \sqrt{\kappa_0} \sin(\sqrt{\kappa_0} L_1) + \cos(\sqrt{\kappa_0} L_1) \right]^2}. \quad (2.38)$$

In the analysis we assumed focusing quadrupoles ($\kappa > 0$); however, the same set of equations can be used for defocusing quadrupoles by just replacing κ_0 with $-\kappa_0$. In

typical experiments, quadrupole and drift lengths are fixed, therefore the projection angle and scaling factor are only functions of the magnet strength κ_0 .

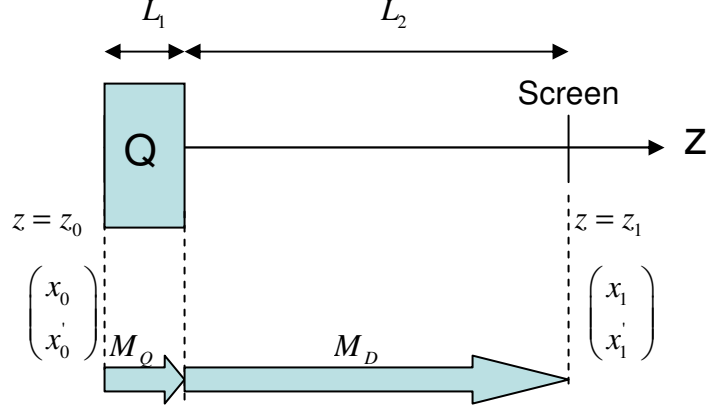


Figure 0.4: Schematic layout of the beamline between z_0 and z_1 . The arrows at the bottom represent the transport matrices.

Filtered projections, Q , at z_1 for different focusing strengths can be used to derive the phase-space distribution. In Fig. 2.5 we show the procedure to obtain those projections for three different magnet settings. First, we have to obtain the beam distribution $g(x, y)$ at z_1 for each case. We can do so by placing an imaging diagnostic there. Figure 2.5 (first row) shows beam distributions $g(x, y)$ at z_1 for three different magnet settings (indicated at the top of the photo). Figure 2.5 (second row) illustrates the corresponding transport matrix, M_1 , (from Eq. 2.36) were we assumed $L_1 = 3.72$ cm, $L_2 = 12.28$ cm and 3.61×10^{-4} G/Acm for the quadrupole length, drift length and field gradient, respectively. From the beam distributions and Eq. 2.26 we calculate the beam profiles $c(x)$ (Fig. 2.5, third row). Now we have to scale those profiles and relate them to the Radon transform of the phase space (see

Eq. 2.34). Our results are demonstrated in the fourth row of Fig. 2.5 as well as the value of the corresponding rotation angle and scaling factor (calculated from Eq. 2.37 and Eq. 2.38). Finally, we have to filter those profiles by using Eq. 2.20. Such profiles are illustrated at the last column of Fig. 2.5. The final step is to integrate over the whole range of angles (Eq. 2.19). As we will show in the next chapter, usually a large number of projections within the whole (0, 180) degree range is necessary to do an accurate reconstruction. In our example we had to collect 87 projections by varying the strength of the magnet from $\kappa_0 = 371.8 \text{ m}^{-2}$ to $\kappa_0 = -230.1 \text{ m}^{-2}$ and our reconstructed phase space is shown in Fig. 2.6.

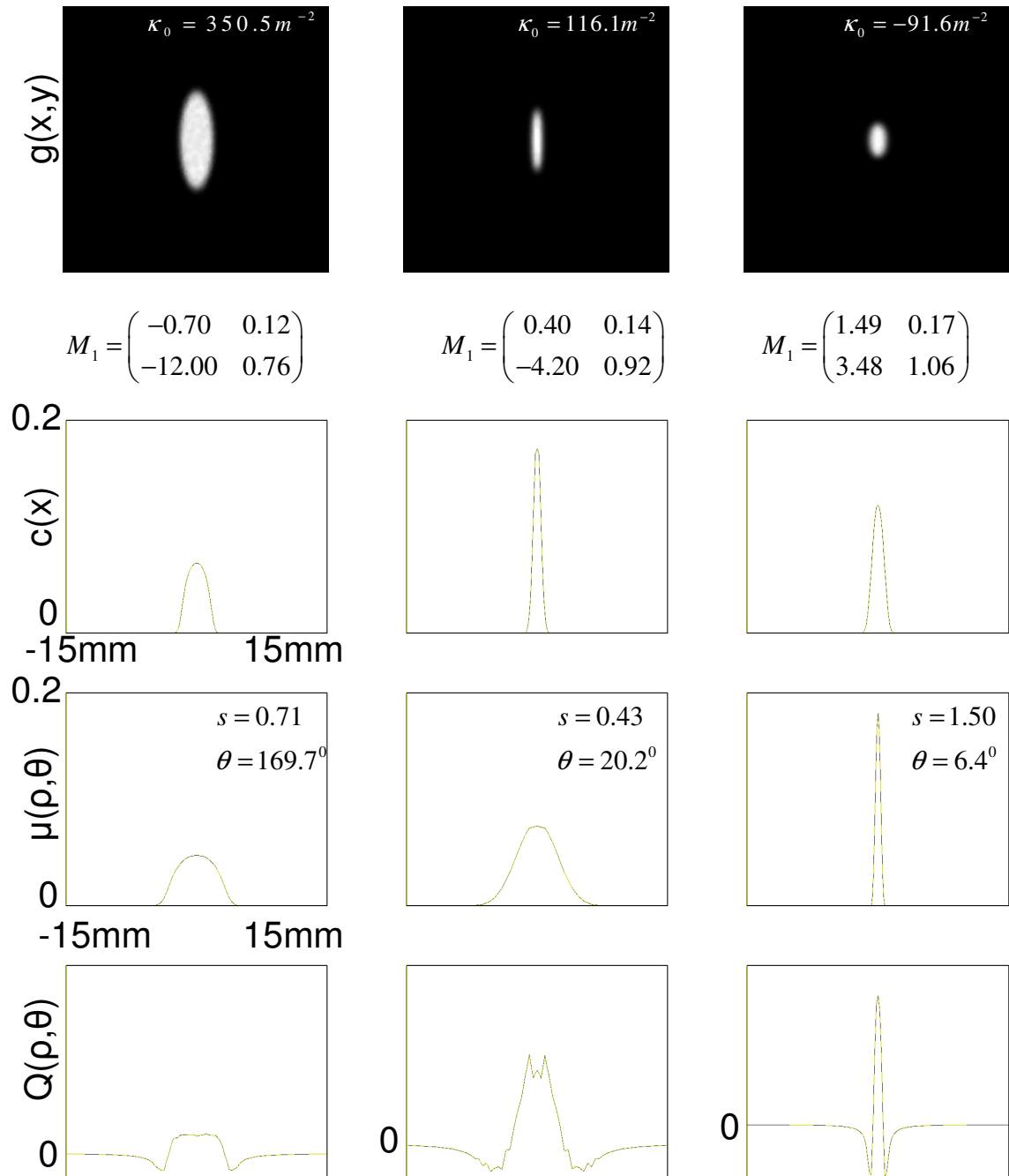


Figure 0.5: Example demonstrating the procedure to obtain projections of the phase-space distribution.

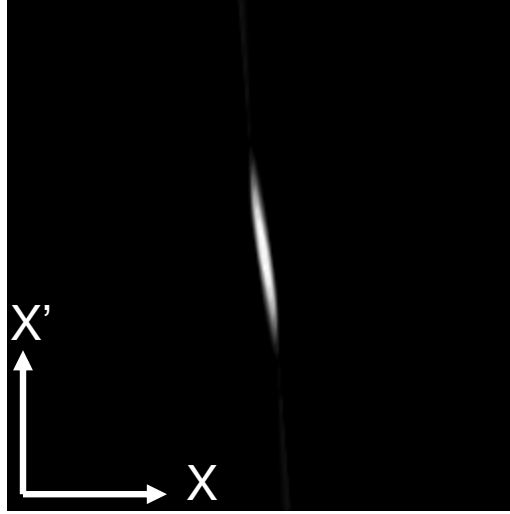


Figure 0.6: Reconstructed phase space at z_0 by processing 87 projections after rotating the phase space by a full 180^0 angle. The intensity parameter was 0.3 and the beam was emittance dominated ($I = 0.6$ mA, $\varepsilon = 6$ μ m).

2.3 Tomography Extension to Beams with Space-Charge

In the previous section we showed that both scaling factor and projection angle can be derived from the beam transport matrix. The analysis was assuming no-space charge. As it is evident from Eq. 2.7 calculation of the transport matrix is complicated in the presence of space charge. The problem is that the space-charge force, in general, depends on the particle distribution and therefore can have very complex functions making the solution of the differential equation very difficult.

In order to simplify the analysis some assumptions need to be made about the density distribution and the resulting space charge forces. One proposed method [25] to calculate the transport matrix is to assume a uniform beam distribution. Then, the

space charge forces become linear and according to Eq. 2.8 the net focusing strengths (generalized to a non-symmetric beam) become [7]:

$$\kappa_x = \kappa_{x0} - \frac{2K}{X(X+Y)}, \quad (2.39)$$

$$\kappa_y = \kappa_{y0} - \frac{2K}{Y(X+Y)}, \quad (2.40)$$

where κ_{x0}, κ_{y0} are quadrupole focusing strengths defined by Eq. 2.5, and X, Y are the $2 \times rms$ beam sizes for x and y directions, respectively. Clearly, when space charge is not significant, only the terms κ_{x0}, κ_{y0} will be used in generating the transfer matrices and the case becomes equivalent to the discussions in Sec 2.2.2; however, for a more intense beam the defocusing space charge terms $-\frac{2K}{X(X+Y)}$ and $-\frac{2K}{Y(X+Y)}$ must be included in the matrix analysis.

In order to obtain the net focusing strength, knowledge of the beam sizes X and Y is needed. In typical experiments it's difficult to place a diagnostic over the desired transport line to get any information of the detailed evolution of X and Y . However, assuming no emittance growth we can calculate the beam envelopes by using Eq 2.10, generalized to non-symmetric distributions and given by [38]

$$X'' + \kappa_{x0}X - \frac{2K}{X+Y} - \frac{\epsilon_x^2}{X^3} = 0, \quad (2.41)$$

$$Y'' + \kappa_{y0}Y - \frac{2K}{X+Y} - \frac{\epsilon_y^2}{Y^3} = 0. \quad (2.42)$$

In order to solve those differential equations we have to assume some initial conditions $(X_0, X'_0, Y_0, Y'_0, \epsilon_x, \epsilon_y)$ at the starting point z_0 . This is a significant difference with the tomography for beams without space-charge (see Sec. 2.2.2) where no such assumption was necessary.

To check the validity of our assumptions we compare at z_1 the calculated from the beam envelope and measured from the screen, beam sizes. In case they do not agree well we adjust the initial conditions and repeat our envelope calculations until we get a better agreement. Once the evolution of X, Y with respect of z is known we calculate the net focusing functions by using Eq. (2.39) and Eq. (2.40). Finally, from Eq. (2.31) and Eq. (2.32) we calculate the scaling factor and the rotation angle, respectively.

The complete beam tomography procedure for beams with space-charge is as follows:

1. Estimate the initial conditions at the starting location z_0 .
2. Identify the correct initial conditions at z_0 : For each magnet setting, solve the beam envelope equations and compare the calculated beam size to that from the measurement. If the two values are not within 10%, estimate new initial conditions and repeat the process until good agreement is achieved.
3. For each magnet setting solve numerically the envelope equation, get $X\{z\}$, $Y\{z\}$ along the beam line at 0.4 mm (or less) steps, and calculate the focusing strength for each step by using Eq. 2.39 and Eq. 2.40.

4. Use those focusing strengths to calculate the transport matrix (for each step) and then obtain the total transport matrix by multiplying those matrices. Now follow the steps 2-5 described in Sec. 2.2.2.
5. Change magnet focusing and repeat steps 3-4.

At the end of the scan integrate the filtered projections, Q , over the rotation angle by using Eq. 2.19.

2.4 Practical Tomography

2.4.1 Limitations

Phase space tomography requires the beam distribution to be rotated to a full 180° angle. Often this cannot be achieved by a single magnet because of several restrictions imposed by the experiment. Such restrictions are listed below:

Beam pipe: The beam size must be kept within a reasonable range when it travels through the accelerator in order to avoid the beam hitting the pipe or possible image-charge effects. Simulations indicate that image forces can have a significant impact on the beam dynamics, since it can cause emittance growth.

Screen size: Tomography relies on the beam distribution captured on the screen. Therefore, the beam size at the measurement point must be controlled to remain within the phosphor screen.

Magnet strength: In practice, the magnet strength is limited by the power supplies or hardware used. For instance, such a restriction can be the magnet current which on UMER cannot exceed ± 3.5 A. Additionally, operating at high quadrupole currents can destroy the quadrupole printed circuit.

Therefore, given those limitations, in some cases one quadrupole is not enough for a full 180^0 rotation of the phase-space. For instance, on UMER we have to employ three and sometimes four quadrupoles to ensure high quality phase spaces. Such configuration not only ensures a full rotation of the phase space but also guarantees that the beam remains far from the beam pipe and therefore the effect of image forces is negligible. Details about the UMER configuration will be discussed in the next section.

2.4.2 Tomography Configuration for UMER

Our tomography configuration on UMER is different than the one used in previous tomography works for two main reasons: First, on UMER, because of the above restrictions (see Se. 2.4.1), we have to use more quadrupoles than other studies which typically employed only one magnet. A schematic layout of the UMER configuration is demonstrated in Fig. 2.7(a). It consists of two sets of altering gradient (FODO) sections. Point A ($z = z_0$) is located at the middle between two UMER quadrupoles and point B ($z = z_1$) is at the location of our imaging diagnostic. The transport matrix consists of five drift matrices and four quadrupole matrices and is given by

$$M_1 = M_{D_5} M_{Q_4} M_{D_4} M_{Q_3} M_{D_3} M_{Q_2} M_{D_2} M_{Q_1} M_{D_1}, \quad (2.43)$$

and is illustrated schematically in Fig. 2.7(b). The particle motion will obey the equation

$$\begin{pmatrix} x_1 \\ y_1 \\ x_1' \\ y_1' \end{pmatrix} = M_1 \begin{pmatrix} x_0 \\ y_0 \\ x_0' \\ y_0' \end{pmatrix}. \quad (2.44)$$

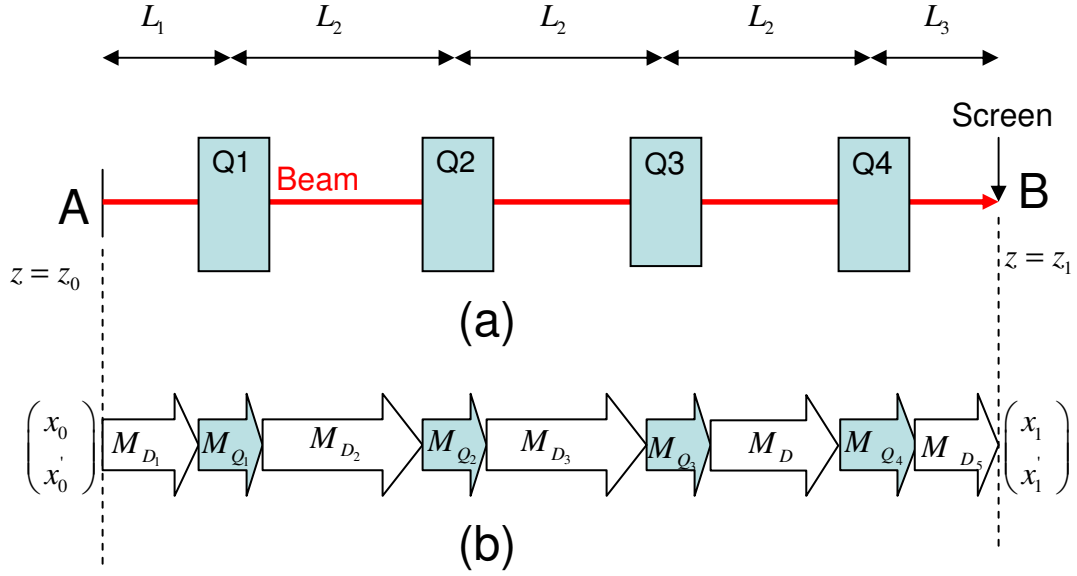


Figure 0.7: Schematic layout of the tomography configuration for UMER; (a) Orientation of quadrupoles; (b) Transfer matrices (indicated by arrows). The distance between A and B is 61.3cm, the distance between A and center of Q1 is $L_1 = 8.0$ cm, the quadrupole center to center distance is $L_2 = 16.0$ cm, and the distance between screen and center of Q4 is $L_3 = 5.3$ cm.

The second different thing of our tomography analysis is the location of the phase space reconstruction. Following the process in Sec. 2.2.2 and using the matrix

of Eq. 2.43 we get knowledge of the phase space $\begin{pmatrix} x_0 \\ y_0 \\ x_0' \\ y_0' \end{pmatrix}$ at point A. This is not always

practical. For example it would be more desirable to reconstruct the phase space at point B since there we have a screen and so we can compare directly the reconstructed phase distribution with the actual beam distribution in configuration space. This phase space can be easily found by projecting the already known phase space at point A by using

$$\begin{pmatrix} x_d \\ x'_d \end{pmatrix} = M_{10} \begin{pmatrix} x_0 \\ x'_0 \end{pmatrix}, \quad (2.45)$$

where M_{10} is transport matrix corresponding to the magnet settings we are interested to get the phase space. We can combine now Eq. 2.44 and Eq. 2.45 and obtain a net transport matrix

$$M_{1,net} = M_1 M_{10}^{-1} \quad (2.46)$$

Therefore, using Eq. 2.46 as our transport matrix in our tomography analysis we can reconstruct the phase spaces at the location of the screen.

2.4.3 Image Processing Requirements

In this section we discuss precautions and requirements while doing image analysis so that we can successfully reconstruct the phase-space distribution.

In our data analysis the beam photos were saved as grayscale images. They consist of i and j spatial coordinates and their respective intensity values (known as *pixels*). They can be thought as 2D matrices, G , where the elements $G(i, j)$ represent the intensity values at a given location (i, j) . The distance between adjacent pixels defines the resolution T (known as mm per pixel for beam photos). The range of the intensities allowed for each pixel is determined by the *bit depth*. For a bit of n , the

pixel has a depth of 2^n . Hence, for 8 bit image, each pixel can have an intensity depth value of 256. The bit rate and resolution are determined by the camera specifications. Obviously, the higher the bit the more details about the image can be seen, however, this increase the computer memory requirement and slows the processing time. For our analysis we vary the bit from 8 to 16. When getting the photos care must be taken regarding the following effects:

Image Saturation While collecting the photos the image brightness can exceed the available intensity range an effect known as *saturation*. Therefore, care must be taken to avoid saturating the images by either decreasing the image brightness or using a camera with higher bit rate.

Image Intensity: The addition of all pixels of an image is known as total intensity. If N is the total number of pixels in i and j directions, then the total intensity is

$$I = \sum_j^N \sum_i^N G(i, j) \quad (2.47)$$

For beams the total image intensity is a measure of the available particles. While varying the magnet strength the numbers of particles have to be conserved. Therefore, a good practice is to measure the intensity of each individual photo after the scan. This might infer information about particle losses or about lens and screen linearity.

Image Centering: Misalignments caused either by the screen or the magnets often can lead to beam offsets. This means that the beam centroid do not match the actual photo center. Therefore, before doing Tomography, a post-centering process is usually necessary after collecting the beam photos in the experiment.

2.4.4 Image Analysis Software

In this section we review the codes we developed for reconstruction and the order we use them in the process. We wrote four MATLAB codes that will: (1) Calculate the transport matrix, scaling factors and rotation angles (Code: ScalF_RotA_Calc.m - see Appendix A1); (2) Center the beam photos and calculate the total intensity (Code: PhotoProcessing.m); (3) Process the beam photos and by using the FBA method reconstruct the phase space (Code: Tomography.m) and (4) Use the phase space to calculate the beam emittance (Code: EmitCalc.m).

We discuss now the procedure we follow and the order we use the above codes to reconstruct the phase space distribution.

Step1: First we generate a table which contains the values of the desired magnet strengths. Next, we run ScalF_RotA_Calc.m:

The code reads those values, solves numerically the beam envelope equations (using Eq. 2.41 and Eq. 2.42), obtains a set of values for $X_i(z)$ and $Y_i(z)$ at a step t and calculates the corresponding focusing strength, $\kappa_{xi}(z)$, by using Eq. 2.39. This is illustrated in Fig. 2.8. Then, by assuming a constant focusing within each step the code gets the transport matrix M_i and finally calculates the net transport matrix by doing a superposition of those matrices ($M_1 = M_{i+2}M_{i+1}M_i \dots$). From the net matrix it calculates the scaling factors and rotation angles for a given set of initial conditions. The output of the code is a table that contains the quadrupole strengths, the resulting

scaling factors and corresponding rotation angles. Same approach applies for the y direction also.

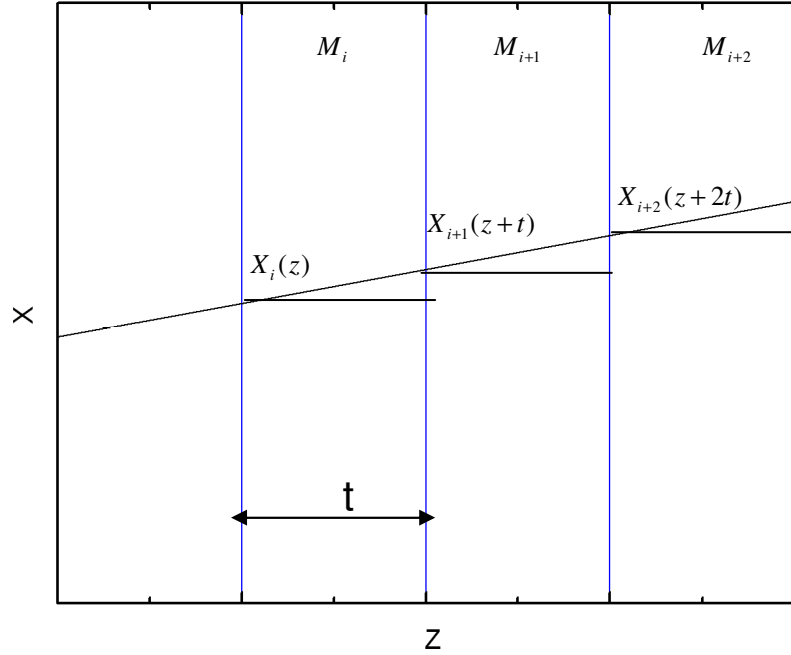


Figure 0.8: Plot shows the numerical solution of the beam envelope equation (Eq. 2.41). Step t should be kept below 0.4 mm and the beam size as well focusing is assumed to be constant within this region.

Step2: Run PhotoProcessing.m:

The code calculates the beam centroid by using the formula:

$$x_c = \sum_i^N \sum_j^N iG(j,i)/I, \quad (2.48)$$

$$y_c = \sum_i^N \sum_j^N jG(j,i)/I. \quad (2.49)$$

where I is the total beam intensity given by Eq. 2.47. Then, it calculates the distance from the photo center $(N/2, N/2)$ and brings the beam photo at that center by doing

the following transforms: $x_c \rightarrow x_c - (x_c - N/2)$ and $y_c \rightarrow y_c - (y_c - N/2)$. After that it saves the new image. Finally, it calculates the total intensity, I , of each photo by using Eq. 2.47 and saves it in a file.

Step3: Run Tomography.m:

The code reads the beam photos created in step 2 and converts it to ASCII-text delimited strings, with each delimiter separating relative pixel intensities. Then by reading the table generated in step 1 it assigns a projection angle and scaling factor to each photo set. Next the program calculates the profiles along x and y and scales them appropriately following the procedure described in Sec. 2.2.2. Finally, it uses those profiles to reconstruct the phase space distribution.

Step4: Run the EmitCalc.m:

The code calculates the $4 \times rms$ unnormalized emittance by using the formula $\epsilon_x = 4\sqrt{\langle x^2 \rangle \langle x'^2 \rangle - \langle xx' \rangle^2}$ (see Sec. 1.1.2). To do so it converts the phase space in Step 3 to ASCII-text delimited strings, with each delimiter separating relative pixel intensities. Then, if N are the number of pixels in vertical and horizontal directions and $M(i, j)$ is the phase space at a point i, j it calculates the second order moments by using the equations

$$\langle x^2 \rangle = T^2 \left[\sum_i^N \sum_j^N i^2 M(j, i) \right] / I, \quad (2.50)$$

$$\langle x'^2 \rangle = T^2 \left[\sum_i^N \sum_j^N j^2 M(j, i) \right] / I \quad (2.51)$$

$$\langle xx' \rangle = T^2 \left[\sum_i^N \sum_j^N (ij) M(j, i) \right] / I, \quad (2.52)$$

were I is the total intensity and T is the spacing between adjacent pixels (in mm/pixel). Then, the total emittance is

$$\epsilon_x = \frac{4T^2}{I} \sqrt{\left[\sum_i^N \sum_j^N i^2 M(j,i) \right] \left[\sum_i^N \sum_j^N j^2 M(j,i) \right] - \left[\sum_i^N \sum_j^N (ij) M(j,i) \right]^2}. \quad (2.53)$$

where we are assuming that the centroid of the phase-space is at the origin.

2.5 Summary

We described the basic theory to apply tomography to reconstruct the beam phase-space. We showed that the technique makes no *a priori* assumptions about the beam distribution when the beam has negligible space-charge. We also extended the technique to beams with space charge. Our approach assumes uniform distributions where the space-charge force becomes linear. Next, we reviewed the tomography magnet configuration for UMER and demonstrated the necessity to use multiple magnets for our reconstruction. Finally, we reviewed the computer codes that we use for our analysis.